Electromagnetic Scattering Interaction Between a Dielectric Cylinder and a Slightly Rough Surface

Tsenchieh Chiu and Kamal Sarabandi
Department of Electrical Engineering and Computer Science
The University of Michigan, Ann Arbor, MI 48109-2122
Tel:(313) 936-1575, Fax:(313) 747-2106
Email: tcchiu@eecs.umich.edu

Abstract – An electromagnetic scattering solution for the interaction between a dielectric cylinder and a slightly rough surface is presented in this paper. Taking the advantage of a newly-developed technique which utilizes the reciprocity theorem, the difficulty in formulating the secondary scattered fields from the composite target reduces to the evaluation of integrals involving the scattered fields from the cylinder and polarization currents of the rough surface induced by a plane wave. Basically, only the current distribution of isolated scatterers are needed to evaluate the interaction in the far-field region. The scattered field from the cylinder is evaluated in the near-field region using a stationary phase approximation along the cylinder axis. Also the expressions for the polarization current induced within the top rough layer of the rough surface derived from the iterative solution of an integral equation are employed in this paper. A sensitivity analysis is performed for determining the dependency of the scattering interaction on the target parameters such as surface rms height, dielectric constant, cylinder diameter and length. It is shown that for nearly vertical cylinders, which is of interest for modeling of vegetation, the cross-polarized backscatter is mainly dominated by the scattering interaction between the cylinder and the rough surface. The accuracy of the theoretical formulation is verified by conducting polarimetric backscatter measurements from a lossy dielectric cylinder above a slightly rough surface. Excellent agreement between the theoretical prediction and experimental results is obtained.

RL-978 = RL-978

List of Figures

1 Configuration of the scattering problem. 19
2 The target is decomposed into two isolated targets above a half-space dielectric: (a) a rough layer of dielectric and (b) a dielectric cylinder. 19
3 The parameters indicating the dimensions and orientation angles for a cylinder. . 20
4 The conical regions of the significant scattered field from a cylinder for the direct incident fields $\mathbf{E}^i_{ed}$ (a) and the reflected incident field $\mathbf{E}^r_{ed}$ (b). 20
5 An inhomogeneous half-space medium with a rough interface. Left side of this figure shows the dielectric profile. 21
6 The RCS ratios of the zeroth-order to the complete first-order for (a) vv-polarized, (b) hh-polarized, and (c) cross-polarized backscatter and for different cylinder tilt angles. The simulation is carried out for a surface with $ks = 0.1$ and $kl = 3.0$. 22
7 The cross-polarized RCS caused by the interaction between a cylinder ($a = 0.385cm$, $l_c = 0.71m$, and $\epsilon_c = 43.4 + i13.2$) and a rough surface ($ks = 0.1$, $kl = 3.0$, and $\epsilon_g = 4.9 + i0.9$). 23
8 The cross-polarized RCS of the cylinder-rough surface composite target versus ks of the rough surface ($a = 0.385cm$, $l_c = 0.71m$, $\epsilon_c = 43.4 + i13.2$, $kl = 3.0$, and $\epsilon_g = 4.9 + i0.9$). 24
9 The cross-polarized RCS of the cylinder-rough surface composite target versus kl of the rough surface ($a = 0.385cm$, $l_c = 0.71m$, $\epsilon_c = 43.4 + i13.2$, $ks = 1.0$, and $\epsilon_g = 4.9 + i0.9$). 24
10 The cross-polarized RCS of the cylinder-rough surface composite target versus the radius of the vertical cylinder ($l_c = 0.71m$, $\epsilon_c = 43.4 + i13.2$, $ks = 0.1$, $kl = 3.0$, and $\epsilon_g = 4.9 + i0.9$). 25
11 The cross-polarized RCS of the cylinder-rough surface composite target versus the length of the vertical cylinder ($a = 0.385cm$, $\epsilon_c = 43.4 + i13.2$, $ks = 0.1$, $kl = 3.0$, and $\epsilon_g = 4.9 + i0.9$). 25
12 The cross-polarized RCS of the cylinder-rough surface composite target versus the height of the cylinder lower end above the ground ($a = 0.385cm$, $l_c = 0.71m$, $\epsilon_c = 43.4 + i13.2$, $ks = 0.1$, $kl = 3.0$, and $\epsilon_g = 4.9 + i0.9$). 26
13 The cross-polarized RCS of the cylinder-rough surface composite target versus the volumetric moisture content of the vertical cylinder ($a = 0.385cm$, $l_c = 0.71m$, $ks = 0.1$, $kl = 3.0$, and $\epsilon_g = 4.9 + i0.9$). 26
14 A comparison of the cross-polarized backscatter of the vertical cylinder-rough surface composite target to that of the rough surface along. The RCS is plotted as a function of incidence angle and number density. The direct backscattering from rough surface alone (σ^0_{pq}) is also plotted for comparison ($a = 0.385cm$, $l_c = 0.71m$, $\epsilon_c = 43.4 + i13.2$, $ks = 0.1$, $kl = 3.0$, and $\epsilon_g = 4.9 + i0.9$). 27
15 The experimental setup for the backscatter measurement of a vertical cylinder above a rough ground plane. 27
16 The backscattering coefficients of the rough surface with $ks = 0.2$ and $kl = 1.0$ at 9.25 GHz. 28
17 The cross-polarized RCS of a water cylinder with $a = 0.83cm$ and $l_c = 11.0cm$ above the rough surface at 9.25 GHz. The RCS of the rough surface alone ($\sigma^0_{pq}A$) is also shown for comparison. 28

1 Introduction

Characterization of scattering behavior of targets above rough surfaces has a number of important practical applications. Assessing the performance of a radar system in detecting a point target in a clutter background like a low-flying aircraft or a military ground-vehicle can be mentioned as one such application. In radar remote sensing of vegetation, accurate scattering models that can describe the interaction of electromagnetic waves and vegetation-covered terrain is of great importance. The common approach is to regard the vegetation-covered surfaces as a random collection of dielectric particles with canonical geometries, such as cylinders representing stems and branches and thin dielectric disks representing leaves, above a half-space dielectric medium with rough interface representing the ground. Most scattering models developed for this problem are based on single scattering properties of the scatterers [1]. In these models, the scattering interaction among the vegetation particles, and the vegetation particles and the rough surface are ignored. In more advanced models, such as radiative transfer [2] (numerical or second-order iterative solutions), the scattering interaction among scatterers are accounted for assuming that the particles are in the far-field of each other. This is not an accurate model because most vegetation structures contain large particles, such as tree trunk, long branches, and the main stems for grasses. The length of these particles are comparable to the vegetation layer thickness and are usually much larger than the wavelength. In these cases the near-field interaction, as opposed to the far-field interaction, must be taken into account [3, 4, 5]. Experimental results indicate that although the first-order scattering models are capable of predicting the co-polarized backscatter adequately, they are not able to predict the cross-polarized backscatter within a desirable accuracy [6].

The underlying ground plane, its dielectric constant and surface roughness play an important role in determining the scattering behavior of a vegetation-covered terrain. Existing scattering models for vegetation account for the interaction between the ground and the other vegetation scatterers by modeling the ground plane as a flat half-space dielectric and using the image theory. The effect of the surface roughness is accounted for by simply modifying the Fresnel reflection coefficient [7]. Therefore the backscatter from an individual scatterer above the ground plane simplifies to four major scattering mechanisms including: 1) the direct backscatter from the target, 2) bistatic scattering from the target reflected from the ground plane, 3) bistatic scattering from the target illuminated by the reflected incident wave, and 4) backscatter from the target illuminated by the reflected wave. Obviously, this solution ignores the near-field interaction between the target and surface roughness which is the subject of the investigation in this paper.

The purpose of this study is to develop an analytical and computationally tractable solution in order to investigate the significance of the interaction between a cylinder and a rough surface. Our approach is based on a recently developed technique which provides the dominant scattering interaction between two arbitrary objects [4]. This approach is very efficient since only the current distribution and scattered fields of isolated scatterers are needed to evaluate the interaction in the far-field region. This method is briefly discussed in section 2.1. In section 2.2, expressions for the scattered fields in the near field region of a tilted dielectric cylinder is provided. In section 2.3, expressions for the polarization currents induced in the top layer of a slightly rough surface with an inhomogeneous dielectric profile are presented. To simplify the calculation a theorem is developed which indicates that in the backscattering direction the near-field interaction of the cylinder with the rough surface is equal to the interaction of the rough surface with the cylinder. This theorem is discussed in the Appendix A. A sensitivity study is carried out and the pertinent results and discussion are provided. Also polarimetric

backscatter measurements are performed at the bistatic scattering facility of the University of Michigan in support of the theoretical model.

2 Theoretical Analysis

Analytical scattering solution that accounts for the near-field interaction between a cylinder and a rough surface is developed in this section. The solution is composed of three basic formulations: 1) the fundamental formulation based on the reciprocity theorem which provides the scattered field, up to the first-order interaction, 2) analytical expansions for the induced current and the scattered field from a dielectric cylinder, and 3) the induced polarization current and the scattered field from a half-space with rough interface. In what follows, the aforementioned formulations are described briefly and then, in section 2.4, are combined to arrive at the desired polarimetric backscattered expressions for the cylinder-rough surface target.

2.1 Electromagnetic Scattering from Two Adjacent Objects

A general method was developed for characterizing scattering interaction between two adjacent target using the scattering properties of the isolated scatterers [4]. In this section we briefly summarize the method and focus on its application to the problem at hand.

Consider two adjacent dielectric objects illuminated by a plane wave. The incident wave would induce a polarization current $\mathbf{J}_1$ in object $\sharp 1$ in the absence of object $\sharp 2$. Considering the volumetric current $\mathbf{J}_1$ as the primary source, this current would induce a volumetric current $\mathbf{J}_{12}$ in the dielectric object $\sharp 2$. The total fields produced in this case, denoted as $\mathbf{E}_1$ and $\mathbf{H}_1$, are the primary scattered fields from object $\sharp 1$ and the secondary scattered field from object $\sharp 2$. In order to compute these fields in the far-field region, consider an an elementary current source $\mathbf{J}_\epsilon$ placed at the observation point illuminating object $\sharp 2$, while the current source $\mathbf{J}_1$ is removed. The elementary current $\mathbf{J}_e = \hat{p}\delta(r - r_o)$ in the presence of object $\sharp 2$ produces an electromagnetic field which will be denoted by $\mathbf{E}_{e2}$ and $\mathbf{H}_{e2}$. The induced current in object $\sharp 2$ with relative permittivity ϵ_2 can be expressed in terms of the total electric field and ϵ_2. The induced polarization in each of the aforementioned cases are given by:

$$\mathbf{J}_{12}(\mathbf{r}) = -ik_0 Y_0(\epsilon_2 - 1)\mathbf{E}_1(\mathbf{r}) , \qquad \mathbf{r} \in V_2, \tag{1}$$

$$\mathbf{J}_{e2}(\mathbf{r}) = -ik_0 Y_0(\epsilon_2 - 1)\mathbf{E}_{e2}(\mathbf{r}) , \qquad \mathbf{r} \in V_2, \tag{2}$$

where k_0 and Y_0 are the wave number and characteristic admittance of free space respectively, and V_2 is the region occupied by object $\sharp 2$. Applying the reaction theorem [14] over the entire space results in

$$\int_{S_\infty} (\mathbf{E}_1 \times \mathbf{H}_{e2} - \mathbf{E}_{e2} \times \mathbf{H}_1) \cdot \hat{n}\, ds = -\int_{V_1} \mathbf{J}_1 \cdot \mathbf{E}_{e2}\, dv - \int_{V_2} \mathbf{J}_{12} \cdot \mathbf{E}_{e2}\, dv + \int_{V_2} \mathbf{J}_{2e} \cdot \mathbf{E}_1\, dv + \hat{p} \cdot \mathbf{E}_1 . \tag{3}$$

Using the radiation condition, it can easily be shown that the integral on the left-hand side vanishes. Also by substituting (1) and (2) into the second and the third integrals on the right-hand side, it can be shown that the last two integrals cancel each other. Therefore, the sum of the primary scattered field from object $\sharp 1$ and the secondary scattered field from object $\sharp 2$ is

given by

$$\hat{p} \cdot \mathbf{E}_1 = \int_{V_1} \mathbf{J}_1 \cdot \mathbf{E}_{e2}\, dv \ . \tag{4}$$

Applying this technique, the scattering formulation for a dielectric cylinder above a slightly rough surface which includes the near-field interaction between the cylinder and the rough surface can be obtained. The geometry of the scattering problem is shown in Fig. 1. By inspection, the backscatter from this composite target can be decomposed into four scattering terms: 1) direct backscatter from the cylinder ($\mathbf{S}^c$), 2) direct backscatter from the rough surface ($\mathbf{S}^r$), 3) cylinder-surface scattering ($\mathbf{S}^{cr}$), and 4) surface-cylinder scattering ($\mathbf{S}^{rc}$). $\mathbf{S}^c$ can be calculated using a semi-exact solution which is based on the eigen-function expansion and physical optics approximation [4]. To calculate $\mathbf{S}^r$, a complete second-order perturbation is applied. Using this method, the scattered fields and induced polarization current of a rough surface with inhomogeneous profile can be calculated as shown in [10]. The challenge here is the calculation of $\mathbf{S}^{cr}$ and $\mathbf{S}^{rc}$. In what follows, analytical expressions for $\mathbf{S}^{rc}$ will be formulated using (4). However, in this approach there are some subtleties involved as one of the two objects is a distributed scatterer. Figures 2(a) and 2(b), respectively, show the geometry of the two isolated scatterers, namely, a rough dielectric slab and a cylinder over a dielectric ground layer. Using the plane wave expansion of the scattered fields and applying reciprocity theorem, it is shown that $S^{cr} = S^{rc}$. Thus employing (4) for calculation of S^{rc}, an expression for the scattered field from the cylinder illuminated by an elementary current (E_{e2}) and the induced polarization current in the top rough layer of the surface illuminated by a plane wave (J_1) are needed.

2.2 Scattered Field from a Tilted Dielectric Cylinder Above a Flat Surface

In this section an expression for the scattered field from a tilted dielectric cylinder above a half-space dielectric layer illuminated by an elementary current (E_{e2}) is obtained. Since the elementary current is in the far-field region of the cylinder, it is assumed that the cylinder is illuminated by a plane wave. The orientation of the cylinder is specified by a unit vector parallel to the cylinder axis given by

$$\hat{\mathbf{c}} = \hat{x} \sin\beta \cos\alpha + \hat{y} \sin\beta \sin\alpha + \hat{z} \cos\beta \ , \tag{5}$$

where β and α are the elevation and azimuth angles of the cylinder respectively, as shown in Fig. 3. Also the center of the cylinder is specified by a position vector $\bar{r}_c = (x_c, y_c, z_c)$.

The radiated field of the elementary current with polarization $\hat{p}$ ($\mathbf{J_e} = \hat{p}\delta(r - r_o)$) in the vicinity of the cylinder, as shown in Fig. 2(b), is approximately given by

$$\mathbf{E}_{ed}(r) = \mathbf{E}^i_{ed}(r) + \mathbf{E}^r_{ed}(r) \ . \tag{6}$$

Here $\mathbf{E}^i_{ed}(r)$ is given by [4]

$$\mathbf{E}^i_{ed}(r) = \frac{-ik_o Z_o}{4\pi r_o} e^{ik_o r_o} e^{-ik_o \hat{k}_s \cdot \mathbf{r}} \hat{k}_s \times \hat{k}_s \times \hat{p} \ , \tag{7}$$

where $-\hat{k}_s$ is the unit vector representing the direction of propagation of $\mathbf{E}^i_{ed}(r)$ and is given by $\hat{k}_s = \hat{x} \sin\theta_s \cos\phi_s + \hat{y} \sin\theta_s \sin\phi_s + \hat{z} \cos\theta_s$. $\mathbf{E}^r_{ed}(r)$ is the field reflected by the surface given by

$$\mathbf{E}^r_{ed}(r) = \frac{ik_o Z_o}{4\pi r_o} e^{ik_o r_o} e^{ik_o \hat{k}^r_s \cdot \mathbf{r}} \left\{ r_v(\theta_s)(\hat{p} \cdot \hat{v}_s)\hat{v}^r_s - r_h(\theta_s)(\hat{p} \cdot \hat{h}_s)\hat{h}^r_s \right\} \ , \tag{8}$$

where $\hat{k}_s^r = -\hat{k}_s + 2(\hat{k}_s \cdot \hat{z})\hat{z}$, $\hat{h}_s^r = (\hat{k}_s^r \times \hat{z})/|\hat{k}_s^r \times \hat{z}|$, $\hat{v}_s^r = \hat{h}_s^r \times \hat{k}_s^r$, and r_v and r_h are the Fresnel reflection coefficients of the ground plane.

Both fields are approximated locally by plane waves. To express the near-zone scattered fields from the cylinder, it is convenient to express the illuminating field in a local coordinate system (x', y', z') in which z'-axis coincides with the cylinder axis. The coordinate transformation between these two systems is simply given by

$$\begin{bmatrix} x \\ y \\ z \end{bmatrix} = \begin{pmatrix} \cos\beta\cos\alpha & -\sin\alpha & \sin\beta\cos\alpha \\ \cos\beta\sin\alpha & \cos\alpha & \sin\beta\sin\alpha \\ -\sin\beta & 0 & \cos\beta \end{pmatrix} \begin{bmatrix} x' \\ y' \\ z' \end{bmatrix} . \tag{9}$$

If we confine our interest in the backscatter direction, that is $\hat{k}^s = -\hat{k}^i$, the propagation direction of incident wave in the new system are given by

$$\hat{k}_i = \hat{x}' \sin\theta_i' \cos\phi_i' + \hat{y}' \sin\theta_i' \sin\phi_i' - \hat{z}' \cos\theta_i' \ , \tag{10}$$

where

$$\cos\theta_i' = \frac{-\hat{k}_i \cdot \hat{\mathbf{c}}}{|\hat{k}_i| \cdot |\hat{\mathbf{c}}|} = -\sin\theta_i \sin\beta \cos(\phi_i - \alpha) + \cos\theta_i \cos\beta \ , \tag{11}$$

$$\sin\theta_i' = \sqrt{1 - \cos^2\theta_i'} \ , \tag{12}$$

$$\cos\phi_i' = [\sin\theta_i \cos\beta \cos(\phi_i - \alpha) + \sin\beta \cos\theta_i] \,/\, \sin\theta_i' \ , \tag{13}$$

$$\sin\phi_i' = \sin\theta_i \sin(\phi_i - \alpha) / \sin\theta_i' \ . \tag{14}$$

Expanding the tangential electric and magnetic fields in terms of eigen-functions of the cylindrical coordinate system and applying the stationary phase approximation only along the direction perpendicular to the cylinder axis [3], the scattered field from the cylinder when illuminated by the $\mathbf{E}_{ed}^i(r)$ in the absence of the top rough layer of the ground plane is given by

$$\mathbf{E}_{ec}^i = \frac{-ik_o Z_o e^{ik_o r_o}}{4\pi r_o} e^{ik_o \hat{k}_i \cdot \bar{\rho}_c} \mathbf{F}^i(\phi' - \phi_i', z') H_0^{(1)}(k_o \sin\theta_i' \rho') \ . \tag{15}$$

Here $\bar{\rho}_c = \hat{x}(x_c - z_c \tan\beta\cos\alpha) + \hat{y}(y_c - z_c \tan\beta \sin\alpha)$, $H_0^{(1)}(\cdot)$ is the zeroth-order Hankel function of the first kind, and

$$\begin{aligned} \mathbf{F}^i(\phi' - \phi_i', z') = \frac{-1}{\sin^2\theta_i'} \sum_{m=-\infty}^{\infty} e^{im(\phi' - \phi_i')} \Bigg\{ & \left[A_m(\hat{k}_c' \times \hat{k}_c' \times \hat{z}') + B_m(\hat{k}_c' \times \hat{z}') \right] e^{ik_{cz}' z'} \\ & + \Bigg[r_v(\theta'') \left(\left[A_m(\hat{k}_c' \times \hat{k}_c' \times \hat{z}') + B_m(\hat{k}_c' \times \hat{z}') \right] \cdot \left(\hat{k}_c' \times \hat{k}_c' \times \hat{n} \right) \right) \frac{\hat{k}_c'' \times \hat{k}_c'' \times \hat{n}}{|\hat{k}_c' \times \hat{k}_c' \times \hat{n}|^2} \\ & + r_h(\theta'') \left(\left[A_m(\hat{k}_c' \times \hat{k}_c' \times \hat{z}') + B_m(\hat{k}_c' \times \hat{z}') \right] \cdot \left(\hat{k}_c' \times \hat{n} \right) \right) \frac{\hat{k}_c'' \times \hat{n}}{|\hat{k}_c' \times \hat{n}|^2} \Bigg] e^{ik_{cz}'' z'} \Bigg\} \ . \end{aligned} \tag{16}$$

For (15) to be valid, two requirements have to be met. First, since the internal polarization currents are assumed to be the same as those of a infinite long cylinder with the same cross-section, the length of the finite cylinder should be electrically long and its dielectric should be somewhat lossy. Second, because of the application of the stationary phase approximation

along the cylinder axis, the observation point must satisfy the far-field criterion in regard with the cylinder diameter, that is

$$\rho > \frac{2d^2}{\lambda} \ . \tag{17}$$

where ρ is the distance between the observation point and the cylinder axis, and d is the cylinder diameter. Accuracy of (15) has been verified by performing polarimetric radar measurements [3] and examining it against the method of moment solution [4, 8].

Equation (16) includes the two components shown in Fig. 4(a). The first component is the bistatic scattered field from the cylinder, which propagates along the direction given by

$$\hat{k}'_c = \hat{x}' \sin\theta'_i \cos\phi' + \hat{y}' \sin\theta'_i \sin\phi' - \hat{z}' \cos\theta'_i \ , \tag{18}$$

And the second term is the reflected scattered field generated by the ground plane, and its direction of propagation is denoted by

$$\hat{k}''_c = \hat{k}'_c - 2(\hat{n} \cdot \hat{k}'_c)\hat{n} \ . \tag{19}$$

The unit vector $\hat{n}$ is the surface normal and is given by

$$\hat{n} = \hat{z} = -\hat{x}' \sin\beta + \hat{z}' \cos\beta \ , \tag{20}$$

and (16) $r_v(\theta'')$ and $r_h(\theta'')$ are the Fresnel reflection coefficients of the ground plane at $\theta'' = \cos^{-1}(-\hat{n} \cdot \hat{k}'_c)$. The coefficients A_m and B_m are given by

$$\begin{aligned} A_m &= C_m^{TM}(\theta'_i)\ \hat{k}_s \times (\hat{k}_s \times \hat{p}) \cdot \hat{z}' + i\bar{C}_m(\theta'_i)\ (\hat{k}_s \times \hat{p}) \cdot \hat{z}' \ , \\ B_m &= C_m^{TE}(\theta'_i)\ (\hat{k}_s \times \hat{p}) \cdot \hat{z}' - i\bar{C}_m(\theta'_i)\ \hat{k}_s \times (\hat{k}_s \times \hat{p}) \cdot \hat{z}' \ , \end{aligned} \tag{21}$$

in which C_m^{TM}, C_m^{TE} and $\bar{C}_m$ are expressed in terms of the cylinder radius, orientation angles, relative permittivity, the frequency, and the incidence angle (see [9]).

It should be noted that $\mathbf{F}^i(\phi' - \phi'_i, z')$ is non-vanishing at observation points for which the stationary point is located on the surface of the finite cylinder, that is, the region of the significant scattered field is confined to the forward scattering cone as shown in Fig. 4(a). The illuminated region (S_i) may be a finite or infinite area, depending on the incidence angle and the orientation angle of the cylinder. If $\theta'_i + \beta \geq 90^o$, then S_i has infinite area. when $\theta'_i + \beta < 90^o$, S_i is an elliptical region (for tilted cylinders) or a circular region (for vertical cylinders).

Similarly, the scattered field from the cylinder when illuminated by the $\mathbf{E}^r_{ed}(r)$ in the absence of the top rough layer of the ground plane is shown in Fig. 4(b). The region of the significant scattered field is confined to the forward scattering cone as well. Noting that the observation points of interest are within the top rough layer, significant scattering exist only when $\theta'_r + \beta > 90^o$. Also the illuminated region S_r, if exist, is always infinite. In this paper, we confine our interest to vertical or nearly vertical cylinders for which $S_r = 0$. Therefore, this mechanism will not be considered in this paper.

2.3 Induced Polarization Current in a Slightly Rough Surface

The expression for the polarization current induced by a plane wave in the top rough layer of a stratified half-space medium is obtained in a recently developed scattering model for slightly rough surface with inhomogeneous dielectric profile [10]. Unlike the traditional small perturbation model (SPM) [11], this new model was developed based on a volume integral in

conjunction with the half-space dyadic Green's function which take into account the effect of dielectric inhomogeneity under the rough surface. This section will only present the formulation required in this paper. The interested readers for the detailed derivation is referred to [10].

Consider an inhomogeneous half-space medium with a rough interface as shown in Fig. 5. It is assumed that the medium is stratified, that is, the relative permittivity is only a function of z, and the permittivity of the top layer down to a depth of d is uniform where $-d < min\{\text{surface profile}\}$. The surface profile is denoted as $\triangle f(x,y)$ where $f(x,y)$ is a zero-mean stationary random process with a known autocorrelation function, and $\triangle$ is a small constant known as the perturbation parameter. The top rough layer is replaced with an equivalent polarization current, and using a volumetric integral equation in conjunction with the dyadic Green's function of the remaining stratified half-space medium, the scattering problem is formulated. Analytical expressions for the induced polarization currents up to any desired order can be derived, nevertheless, in this treatment, only the induced polarization current up to the second-order are needed. That is, the total polarization current is approximated by:

$$\mathbf{J}(\mathbf{r}) = \mathbf{J}_0(\mathbf{r}) + \triangle \mathbf{J}_1(\mathbf{r}) + \triangle^2 \mathbf{J}_2(\mathbf{r}) \ . \tag{22}$$

These currents are expressed in term of their two-dimensional Fourier transforms defined by

$$\mathbf{J}_n(\mathbf{r}) = \frac{1}{(2\pi)^2} \int \tilde{\mathbf{J}}_n(\mathbf{k}_\perp, z) e^{i\mathbf{k}_\perp \bar{\rho}} \, d\mathbf{k}_\perp \ , \tag{23}$$

in a recursive manner. The expression for $\tilde{\mathbf{J}}_0(\mathbf{k}_\perp, z)$ is given by

$$\tilde{\mathbf{J}}_0(\mathbf{k}_\perp, z) = (2\pi)^2 \delta(\mathbf{k}_\perp - \mathbf{k}_\perp^i) \mathbf{J}_0(z) = (2\pi)^2 \delta(\mathbf{k}_\perp - \mathbf{k}_\perp^i) \left[J_{oh}(z) \hat{h}(k_z^i) + J_{ot}(z) \hat{t}(k_z^i) + J_{oz}(z) \hat{z} \right] \ , \tag{24}$$

where $\hat{h}(k_z^i) = (\hat{k}_i \times \hat{z})/|\hat{k}_i \times \hat{z}|$, $\hat{t}(k_z^i) = \hat{z} \times \hat{h}(k_z^i)$, and

$$\begin{aligned}
J_{0h}(z) &= -i \frac{2k_0 k_z^i}{k_z^i + k_{1z}^i} Y_0 (\epsilon - 1) \, C_0^h(\mathbf{k}^i, z) \left[\mathbf{E}_o \cdot \hat{h}(k_z^i) \right] e^{-ik_z^i d} \ , \\
J_{0t}(z) &= -i \frac{2k_0 k_z^i k_{1z}^i}{k_\rho^i \left(\epsilon k_z^i + k_{1z}^i \right)} Y_0 (\epsilon - 1) \, C_0^v(\mathbf{k}^i, z) \left[\mathbf{E}_o \cdot \hat{z} \right] e^{-ik_z^i d} \ , \\
J_{0z}(z) &= -i \frac{2k_0 k_z^i}{\epsilon k_z^i + k_{1z}^i} Y_0 (\epsilon - 1) \, C_1^v(\mathbf{k}^i, z) \left[\mathbf{E}_o \cdot \hat{z} \right] e^{-ik_z^i d} \ ,
\end{aligned}$$

The parameters in these expressions for the zeroth-order current are given by

$$\begin{aligned}
k_{1z}^i &= k_0 \sqrt{\epsilon - \sin^2 \theta_i} \, , \qquad k_\rho^i = k_0 \sin \theta_i \, , \qquad R_h^i = \frac{k_z^i - k_{1z}^i}{k_z^i + k_{1z}^i} \, , \qquad R_v^i = \frac{\epsilon k_z^i - k_{1z}^i}{\epsilon k_z^i + k_{1z}^i} \, , \\
C_n^h(\mathbf{k}, z) &= \frac{(-1)^n \left(R_h - r_h \right) e^{ik_{1z} z} + \left(R_h r_h - 1 \right) e^{-ik_{1z} z}}{R_h \left(R_h - r_h \right) e^{ik_{1z} d} + \left(R_h r_h - 1 \right) e^{-ik_{1z} d}} \ , \\
C_n^v(\mathbf{k}, z) &= \frac{(-1)^n \left(r_v - R_v \right) e^{ik_{1z} z} + \left(R_v r_v - 1 \right) e^{-ik_{1z} z}}{R_v \left(R_v - r_v \right) e^{ik_{1z} d} + \left(R_v r_v - 1 \right) e^{-ik_{1z} d}}
\end{aligned}$$

As before r_h and r_v denotes the Fresnel reflection coefficients of the half-space medium. The

expressions for higher order currents are similar to that of the zeroth order, and are given by

$$\tilde{J}_{Nh}(\mathbf{k}_\perp, z) = \frac{ik_0^2(\epsilon-1)}{k_z + k_{1z}} C_0^h(\mathbf{k}, z) \left[\tilde{\mathbf{V}}_N \cdot \hat{h}(k_z)\right] ,$$
$$\tilde{J}_{Nt}(\mathbf{k}_\perp, z) = \frac{ik_0 k_{1z}(\epsilon-1)}{\epsilon k_z + k_{1z}} C_0^v(\mathbf{k}, z) \left[\tilde{\mathbf{V}}_N \cdot \hat{v}(-k_z)\right] ,$$
$$\tilde{J}_{Nz}(\mathbf{k}_\perp, z) = \frac{ik_0 k_\rho(\epsilon-1)}{\epsilon k_z + k_{1z}} C_1^v(\mathbf{k}, z) \left[\tilde{\mathbf{V}}_N \cdot \hat{v}(-k_z)\right] ,$$

where

$$\tilde{\mathbf{V}}_N = \sum_{n=0}^{N-1} \sum_{m=0}^{N-n-1} \frac{\binom{N-n-1}{m}(ik_z)^m}{(N-n)!} \cdot \left[\frac{\partial^{N-n-m-1}}{\partial (z')^{N-n-m-1}} \tilde{\mathbf{J}}_n(\mathbf{k}_\perp, d)\right] * \overset{N-n}{\bigotimes} F(\mathbf{k}_\perp) .$$

Here $\overset{n}{\bigotimes}$ denotes the n-fold self-convolution operator ($\overset{n}{\bigotimes} F = \overbrace{F * F * \cdots * F}^{n}$).

2.4 Evaluation of the Secondary Scattered Field

Substituting (15) and (22) into (4), the secondary scattered field from the cylinder is given by

$$\hat{p} \cdot \mathbf{E}_s^{rc} = \iint_{S_t'} dxdy \int_0^{d+\Delta f(x,y)} \mathbf{J}(\mathbf{r}) \cdot \mathbf{E}_{ec}^i(\bar{\rho}, z)\, dz . \tag{25}$$

It is noted that $\mathbf{E}_{ed}^i$ and $\mathbf{E}_{ed}^r$ are not included in (25), since these fields would produce the direct backscatter from the rough surface. For surface with small rms height $\Delta f(x,y)$ is a small quantity, and therefore (25) can be approximately by

$$\hat{p} \cdot \mathbf{E}_s^{rc} = \iint_{S_t'} dxdy \int_0^d \mathbf{J}(\mathbf{r}) \cdot \mathbf{E}_{ec}^i(\bar{\rho}, z)\, dz + \sum_{n=0}^{\infty} \iint_{S_t'} \frac{[\Delta f(x,y)]^{n+1}}{(n+1)!} \frac{\partial^n}{\partial z^n} \left\{\mathbf{J}(\mathbf{r_d}) \cdot \mathbf{E}_{ec}^i(\bar{\rho}, d)\right\} dxdy , \tag{26}$$

where $\mathbf{r_d} = \hat{x}x + \hat{y}y + \hat{z}d$. Substituting (23) into (26), the first-order secondary scattered field can be expressed as:

$$\hat{p} \cdot \mathbf{E}_s^{rc(1)} = \frac{\Delta}{(2\pi)^2} \int_0^d dz \int_{-\infty}^{\infty} \tilde{\mathbf{J}}_1(\mathbf{k}_\perp, z) \iint_{S_t} \mathbf{E}_{ec}^i(\bar{\rho}, z) e^{i\mathbf{k}_\perp \bar{\rho}}\, ds\, d\mathbf{k}_\perp$$
$$+ \frac{\Delta}{(2\pi)^2} \mathbf{J}_0(d) \int_{-\infty}^{\infty} F(\mathbf{k}_\perp - \mathbf{k}_\perp^i) \iint_{S_t} \mathbf{E}_{ec}^i(\bar{\rho}, d) e^{i\mathbf{k}_\perp \bar{\rho}}\, ds\, d\mathbf{k}_\perp . \tag{27}$$

Similarly, the second-order secondary scattered field is given by:

$$\hat{p}\cdot\mathbf{E}_s^{rc(2)} = \left(\frac{\triangle}{2\pi}\right)^2 \int_0^d dz \int_{-\infty}^{\infty} \tilde{\mathbf{J}}_2(\mathbf{k}_\perp, z) \iint_{S_t} \mathbf{E}_{ec}^i(\bar{\rho}, z) e^{i\mathbf{k}_\perp \bar{\rho}}\, ds\, d\mathbf{k}_\perp$$
$$+ \left(\frac{\triangle}{2\pi}\right)^2 \int_{-\infty}^{\infty} F(\mathbf{k}_\perp) \star \tilde{\mathbf{J}}_1(\mathbf{k}_\perp, d) \iint_{S_t} \mathbf{E}_{ec}^i(\bar{\rho}, d) e^{i\mathbf{k}_\perp \bar{\rho}}\, ds\, d\mathbf{k}_\perp$$
$$+ \left(\frac{1}{2\pi}\right)^2 \frac{\triangle^2}{2} \mathbf{J}_0(d) \int_{-\infty}^{\infty} F(\mathbf{k}_\perp) \star F(\mathbf{k}_\perp - \mathbf{k}_\perp^i) \iint_{S_t} \frac{\partial}{\partial z} \mathbf{E}_{ec}^i(\bar{\rho}, d) e^{i\mathbf{k}_\perp \bar{\rho}}\, ds\, d\mathbf{k}_\perp$$
$$+ \left(\frac{1}{2\pi}\right)^2 \frac{\triangle^2}{2} \frac{d}{dz} \mathbf{J}_0(d) \int_{-\infty}^{\infty} F(\mathbf{k}_\perp) \star F(\mathbf{k}_\perp - \mathbf{k}_\perp^i) \iint_{S_t} \mathbf{E}_{ec}^i(\bar{\rho}, d) e^{i\mathbf{k}_\perp \bar{\rho}}\, ds\, d\mathbf{k}_\perp \ . \quad (28)$$

Note that for evaluating the zeroth-order secondary scattered field, one can simply use the formulation derived for a cylinder above a smooth ground plane.

The polarimetric response of a target can be expressed in terms of its complex scattering matrix defined as

$$\mathbf{E}^s = \frac{e^{ikr}}{r} \bar{\bar{\mathbf{S}}}\, \mathbf{E}^i \ .$$

For random targets, the expected radar cross section for a particular transmit and receive polarization configuration can be calculated from

$$\sigma_{pqpq} = 4\pi \langle |S_{pq}|^2 \rangle \ , \qquad p, q \in \{h, v\} \, , \quad (29)$$

where $\langle \cdot \rangle$ denotes ensemble averaging. Depending on the order of the scattered field, $\mathbf{S}^{rc}$ can also be expanded in terms of a perturbation series, i.e., $\mathbf{S}^{rc} \approx \mathbf{S}^{rc(0)} + \triangle \mathbf{S}^{rc(1)} + \triangle^2 \mathbf{S}^{rc(2)}$. As mentioned earlier, $\mathbf{S}^{rc(0)}$ can easily be obtained from

$$S_{pq}^{rc(0)} = r_p(\theta_i)\, S_{pq}^{cyl}(\hat{k}_r, \hat{k}_s) e^{ik_o(\hat{k}_r - \hat{k}_s)\cdot \bar{r}_c} \ . \quad (30)$$

Here $r_p(\theta_i)$ is the reflection coefficient of the ground plane and the top rough layer with a flat interface ($\triangle = 0$), $\hat{k}_r = \hat{k}_i - 2(\hat{k}_i \cdot \hat{n})\hat{n}$, and S_{pq}^{cyl} denotes a bistatic scattering matrix element of the cylinder located at the origin in free space which can be evaluated by using the infinite-cylinder approximation [13]. Expressions for $\mathbf{S}^{rc(1)}$ and $\mathbf{S}^{rc(2)}$ can be obtained from (27) and (28), respectively. The calculation of $\mathbf{S}^{cr}$ directly is even more complicated than $\mathbf{S}^{rc}$. It can be shown that $\mathbf{S}^{cr}$ can be evaluated from $\mathbf{S}^{rc}$ using $\bar{\bar{\mathbf{S}}}^{cr} = [\bar{\bar{\mathbf{S}}}^{rc}]^{(-t)}$, that is

$$\begin{pmatrix} S_{vv}^{cr} & S_{vh}^{cr} \\ S_{hv}^{cr} & S_{hh}^{cr} \end{pmatrix} = \begin{pmatrix} S_{vv}^{rc} & -S_{hv}^{rc} \\ -S_{vh}^{rc} & S_{hh}^{rc} \end{pmatrix} \ . \quad (31)$$

Here the superscript $(-t)$ denotes the matrix transposing and multiplying the off-diagonal elements by -1. The proof of this identity is presented in Appendix A.

Finally an analytical expression for the average RCS of the cylinder-rough surface composite target illuminated by a collimated beam, illuminating an area A of the rough surface, is given

by

$$\frac{\sigma_{pqpq}}{4\pi} = |S^c_{pq} + S^{rc(0)}_{pq} + S^{cr(0)}_{pq}|^2 + \langle |S^{rc(1)}_{pq} + S^{cr(1)}_{pq}|^2 \rangle \triangle^2$$
$$+ 2\,Re\left\{ \langle S^{r(1)}_{pq} (S^{rc(1)}_{pq} + S^{cr(1)}_{pq})^* \rangle + (S^c_{pq} + S^{rc(0)}_{pq} + S^{cr(0)}_{pq}) \langle (S^{rc(2)}_{pq} + S^{cr(2)}_{pq}) \rangle^* \right\} \triangle^2$$
$$+ \sigma^{r0}_{pqpq} \frac{A}{4\pi} \,. \qquad p, q \in \{h, v\} \,. \tag{32}$$

The first term in (32) represents the zero-order solution, and the second term accounts for the first-order secondary scattered field. The third term in (32) represents the coherent interaction of the cylinder and rough surface scattered fields. The complete second-order backscattering coefficient from the rough surface along is represented by the fourth term of (32) and is given by

$$\sigma^{r0}_{pqpq} = \lim_{A\to\infty} \frac{4\pi}{A} \left\{ \left\langle |S^{r(1)}_{pq}|^2 \right\rangle \triangle^2 + \left[\left\langle |S^{r(2)}_{pq}|^2 \right\rangle + 2Re \left\langle S^{r(1)}_{pq} S^{r(3)*}_{pq} \right\rangle \right] \triangle^4 , \right\} \tag{33}$$

where $S^{r(1)}_{pq}$, $S^{r(2)}_{pq}$, and $S^{r(3)}_{pq}$ are the first-, second-, and third-order backscatter of the the rough surface. The expressions for $S^{r(1)}_{pq}$ are given by

$$S^{r(1)}_{hh} = \frac{k_0^2 k^i_z k^s_z (\epsilon - 1) e^{-i(k^i_z + k^s_z)d}}{\pi (k^i_z + k^i_{1z})(k^s_z + k^s_{1z})} C^h_0(\mathbf{k}^s, d) C^h_0(\mathbf{k}^i, d) \cos(\phi_s - \phi_i) F(\mathbf{k}^s_\perp - \mathbf{k}^i_\perp) \,, \tag{34}$$

$$S^{r(1)}_{hv} = \frac{k_0 k^i_z k^s_z k^i_{1z} (\epsilon - 1) e^{-i(k^i_z + k^s_z)d}}{\pi (\epsilon k^i_z + k^i_{1z})(k^s_z + k^s_{1z})} C^h_0(\mathbf{k}^s, d) C^v_0(\mathbf{k}^i, d) \sin(\phi_s - \phi_i) F(\mathbf{k}^s_\perp - \mathbf{k}^i_\perp) \,, \tag{35}$$

$$S^{r(1)}_{vh} = \frac{k_0 k^i_z k^s_z k^s_{1z} (\epsilon - 1) e^{-i(k^i_z + k^s_z)d}}{\pi (\epsilon k^s_z + k^s_{1z})(k^i_z + k^i_{1z})} C^h_0(\mathbf{k}^i, d) C^v_0(\mathbf{k}^s, d) \sin(\phi_s - \phi_i) F(\mathbf{k}^s_\perp - \mathbf{k}^i_\perp) \,, \tag{36}$$

$$S^{r(1)}_{vv} = \frac{k^i_z k^i_{1z} (\epsilon - 1) e^{-i(k^i_z + k^s_z)d}}{\pi (\epsilon k^i_z + k^i_{1z})(\epsilon k^s_z + k^s_{1z})} \left[-k^s_z k^s_{1z} C^v_0(\mathbf{k}^s, d) C^v_0(\mathbf{k}^i, d) \cos(\phi_s - \phi_i) + \frac{\epsilon k^s_z k^s_\rho k^i_\rho}{k^i_{1z}} \right.$$
$$\left. \cdot C^v_1(\mathbf{k}^s, d) C^v_1(\mathbf{k}^i, d) \right] F(\mathbf{k}^s_\perp - \mathbf{k}^i_\perp) \,, \tag{37}$$

where $F(\cdot)$ is the Fourier transform of the surface roughness ($f(\cdot)$), and the rather lengthy expressions for $S^{r(2)}_{pq}$ and $S^{r(3)}_{pq}$ can be found in [10, 12]. For a distributed target composed of uniformly distributed cylinders with a number density N above a rough surface, the scattering coefficients can be computed from:

$$\frac{\sigma^0_{pqpq}}{4\pi} = N \left\{ |S^c_{pq} + S^{rc(0)}_{pq} + S^{cr(0)}_{pq}|^2 + \langle |S^{rc(1)}_{pq} + S^{cr(1)}_{pq}|^2 \rangle \triangle^2 + 2\,Re \left\{ \langle S^{r(1)}_{pq} (S^{rc(1)}_{pq} + S^{cr(1)}_{pq})^* \rangle \right.\right.$$
$$\left.\left. + (S^c_{pq} + S^{rc(0)}_{pq} + S^{cr(0)}_{pq}) \langle (S^{rc(2)}_{pq} + S^{cr(2)}_{pq}) \rangle^* \right\} \triangle^2 \right\} + \frac{\sigma^{r0}_{pqpq}}{4\pi} \,, \qquad p, q \in \{h, v\} \,, \tag{38}$$

where the mutual interaction between cylinders is ignored.

To evaluate the ensemble average in (32) some properties of Gaussian processes can be applied. For example if $F(\mathbf{k}_\perp)$ appears as a multiplicative factor, such as those in (34), (35), (36), and (37), then the following definition can be used:

$$\lim_{A\to\infty} \frac{1}{A} \left\langle \left| \triangle F(\mathbf{k}^s_\perp - \mathbf{k}^i_\perp) \right|^2 \right\rangle = W(\mathbf{k}^s_\perp - \mathbf{k}^i_\perp) \,, \tag{39}$$

where $W(\mathbf{k}_\perp)$ is the power spectral density of the surface. For some expressions $F(\mathbf{k}_\perp)$ appears inside an integration and therefore the evaluation of $\langle F(\mathbf{k}_\perp)F^*(\mathbf{k}'_\perp)\rangle$ is required. In such cases the following identity can be used [2]:

$$\triangle^2\langle F(\mathbf{k}_\perp)F^*(\mathbf{k}'_\perp)\rangle = (2\pi)^2\,\delta(\mathbf{k}_\perp - \mathbf{k}'_\perp)W(\mathbf{k}_\perp)\,. \tag{40}$$

which simplifies the evaluation of a two-fold integration. Other useful properties needed for the evaluation of the ensemble averages can be found in [10].

A particular case of interest is when the cylinder axis is vertical to the mean surface. In this case the cross-polarized backscatter is mainly generated from the interaction between the cylinder and the rough surface and the rough surface itself. In this case $S_{vh}^{r(1)}$, $S_{vh}^{rc(0)}$, $S_{vh}^{cr(0)}$,and S_{vh}^{c} are zero, and the expression for the cross-polarized RCS is simplified to

$$\sigma_{vhvh} = 4\pi\langle|S_{vh}^{rc(1)} + S_{vh}^{cr(1)}|^2\rangle\triangle^2 + \sigma^{or}{}_{vhvh}A\ , \tag{41}$$

where the expressions for $S_{vh}^{rc(1)}$ and $S_{vh}^{cr(1)}$ are given in [12], and the expression for the cross-polarized backscattering coefficient is given by

$$\begin{aligned}\sigma^{or}{}_{hvhv} = \sigma^{or}{}_{vhvh} = \frac{\left|k_0 k_z^i(\epsilon-1)^2\right|^2}{16\pi^3}\left|\left(1-R_v^i\right)\left(1+R_h^i\right)C_0^h(\mathbf{k}^i,d)C_0^v(\mathbf{k}^i,d)\right|^2 \\ \cdot\int_{-\infty}^{\infty} W(\mathbf{k}_\perp-\mathbf{k}_\perp^i)W(\mathbf{k}_\perp+\mathbf{k}_\perp^i)\sin^2(\phi-\phi_i)\cos^2(\phi-\phi_i) \\ \cdot\left|\frac{k_0^2}{k_z+k_{1z}}C_0^h(\mathbf{k},d) - \frac{k_z k_{1z}}{k_{1z}+\epsilon k_z}C_0^v(\mathbf{k},d)\right|^2 d\mathbf{k}_\perp\ ,\end{aligned} \tag{42}$$

At low frequencies or for electrically thin cylinders, the Rayleigh solution or only the zeroth-order component in (16) corresponding to $m = 0$ is sufficient to calculate $\mathbf{E}_{ec}$. In this case, S_{vh}^{rc} and S_{hv}^{rc} are respectively given by

$$\begin{aligned}S_{vh}^{rc} = \frac{\triangle Z_o k_o}{(2\pi)^2}e^{ik_o(\hat{\mathbf{k}}_i-\hat{\mathbf{k}}_s)\cdot\bar{\rho}_c}C_0^{TM}J_{0h}(d)\Bigg\{\cos\theta_s\int\Bigg[\frac{\left(e^{-ik_z^s d}-1+r_v^s(e^{ik_z^s d}-1)\right)}{k_z^s}\frac{k_z k_{1z}(\epsilon-1)}{k_{1z}+\epsilon k_z} \\ +\left(e^{-ik_z^s d}-r_v^s e^{ik_z^s d}\right)\Bigg]F(\mathbf{k}_\perp-\mathbf{k}_\perp^i)\sin\phi_k B_1(\mathbf{k}_\perp)\,d\mathbf{k}_\perp \\ -i\sin\theta_s\int\frac{\left(e^{-ik_z^s d}-1-r_v^s(e^{ik_z^s d}-1)\right)}{k_z^s}\frac{k_z k_{1z}(\epsilon-1)}{k_{1z}+\epsilon k_z}F(\mathbf{k}_\perp-\mathbf{k}_\perp^i)\sin\phi_k B_2(\mathbf{k}_\perp)\,d\mathbf{k}_\perp\ ,\Bigg\}\end{aligned} \tag{43}$$

$$\begin{aligned}S_{hv}^{rc} = \frac{\triangle Z_o k_o k_z^s}{(2\pi)^2}\epsilon^{ik_o(\hat{\mathbf{k}}_i-\hat{\mathbf{k}}_s)\cdot\bar{\rho}_c}C_0^{TE}J_{0t}(d)\cdot\int\Bigg[\frac{\left(e^{-ik_z^s d}-1-r_h^s(e^{ik_z^s d}-1)\right)}{k_z^s}\frac{k_o^2(\epsilon-1)}{k_{1z}+\epsilon k_z} \\ +\left(e^{-ik_z^s d}+r_h^s e^{ik_z^s d}\right)\Bigg]F(\mathbf{k}_\perp-\mathbf{k}_\perp^i)\sin\phi_k B_1(\mathbf{k}_\perp)\,d\mathbf{k}_\perp\ ,\end{aligned} \tag{44}$$

where

$$B_1(\mathbf{k}_\perp) = \int_{a+h\tan\theta_t}^{a+(l_c+h)\tan\theta_t} H_0^{(1)}(k_o \sin\theta^s \rho') J_0'(|\mathbf{k}_\perp|\rho')\rho' d\rho' \ ,$$

$$B_2(\mathbf{k}_\perp) = \int_{a+h\tan\theta_t}^{a+(l_c+h)\tan\theta_t} H_0^{(1)}(k_o \sin\theta^s \rho') J_0(|\mathbf{k}_\perp|\rho')\rho' d\rho' \ .$$

3 Simulation and Experimental Data Analysis

In this section a sensitivity analysis is presented to demonstrate the significance of the scattering interaction between cylinders and rough surfaces to the overall backscatter. Also polarimetric backscatter measurement that demonstrates the validity of the scattering formulation are presented.

We begin the sensitivity analysis with a realistic scenario. Consider a soybean plant above a ground plane with a slightly rough interface. The scattering interaction between the main stem of the plant and the rough surface is of interest. Typical values of $0.71m$ and $0.385cm$ are chosen for the length and radius of the main stem respectively, and the simulation is performed at 1.25 GHz. The length of the main stem is 2.96λ, and the ratio of the length to the radius is 184.4. For these dimensions the far-field criterion given by (17) requires that $\rho > 0.048$ cm. Hence for most practical situation (15) is valid. The dielectric constant of a stem with moisture constant $m_v = 0.58$ is found to be $43.4 + i13.2$ at 1.25 GHz [18]. The cylinder, which is used to model the main stem of the soybean, is placed right above the rough surface with $ks = 0.1$ and $kl = 3.0$ having an exponential correlation function. The volumetric soil moisture content is set to be 0.1, and the dielectric constant is calculated by applying an empirical model [15] choosing a soil texture with 10% sand and 30% clay. Figures 6 shows the RCS ratio of the zeroth-order (the first term in (32)) to the complete first-order backscattering solution excluding the direct backscatter from the rough surface (the first three terms in (32)) is plotted versus incidence angle. The RCSs are calculated and averaged over many azimuthal angles (α) for six different cylinder tilt angles (β): 2^o, 4^o, 6^o, 8^o, 10^o, and 12^o. In this simulation azimuthal symmetry (uniform distribution over α) is assumed. Figure 6(a) and Fig. 6(b) show that, for the co-polarized backscatter, the average of the zeroth-order solution is sufficient except when the incidence angle is close to normal incidence. On the other hand, Fig. 6(c) shows that the cylinder-rough surface interaction is significant for the cross-polarized scattering, especially for nearly vertical cylinders. The simulation for the vertical cylinder corresponding to $\beta = 0^o$ is not plotted here, because the zeroth-order solution predicts no cross-polarized backscatter. As the tilt angle increases, the cross-polarized backscatter predicted by the zeroth-order solution increases, and therefore the cylinder-rough surface interaction becomes less important.

It should be noted here that the numerical evaluations of the integrals which account for the interaction between the cylinder and rough surface is much more time-consuming for a tilted cylinder than for a vertical cylinder. The reason for this is that the lit area, shown in Fig. 4(a), has a circular contour when the cylinder is vertical and the integration along ϕ can be carried out analytically. For tilted cylinder the contour is elliptical and four-fold numerical integrations must be carried out. Besides, for tilted cylinders an averaging over the azimuthal angle α is required. On a Sun workstation Ultra 2, while it takes only less that 10 second to evaluate the scattering interaction for a vertical cylinder, it takes about 15 to

130 minutes for a tilted cylinder, depending on the incidence angle. As mentioned earlier the interaction between cylinders and rough surfaces become less important as the cylinders' tilt angle increases. Therefore, the focus in the rest of simulations will be on the cross-polarized backscatter for nearly vertical cylinders, which is often a case of interest in problems such as scattering from vegetation canopies. The complete first-order cross-polarized RCS (the first three terms in (32)) of the example shown in Fig. 6 is presented in Fig. 7. It is shown that the scattering interaction increases with the increase in the incidence angle and the cylinder's tilt angle. It is also shown that for $\beta \leq 6^o$ the cross-polarized RCS can be approximated well by that of the vertical cylinder.

The effect of surface roughness parameters (ks and kl) on the cross-polarized RCS of the vertical cylinder and rough surface is also examined. The direct backscatter from rough surface is still excluded in this investigation to focus on the interaction between these two targets, so the RCS will only include the first term in (41). In Fig. 8 the correlation length is kept constant ($kl = 3.0$) while the surface rms height is varied. It is found that the cross-polarized RCS is rather sensitive to the variation of ks. In Fig. 9, the rms height is kept constant ($ks = 0.1$) and the correlation length is varied. It is shown that the sensitivity to kl diminishes when when $kl > 1.5$.

Figure 10 shows the cross-polarized RCS (only the first term in (41)) of the vertical cylinder and rough surface as a function of the cylinder radius. In this simulation the cylinder length and dielectric constant are, respectively, $0.71m$ and $\epsilon = 43.4 + i13.2$, and the surface parameters are $ks = 0.1$ and $kl = 3.0$. When the cylinder is electrically thin ($ka\sqrt{|\epsilon|} << 1$) the cross-polarized RCS can be calculated using (43) and (44), which indicates that the cross-polarized RCS varies as $(ka)^4$. As ka increase further, the cross-polarized RCS begins to oscillate, and exhibits a much gentler rate of increase with increasing ka. Figure 11 shows the dependency of the cross-polarized RCS (only the first term in (41)) on the vertical cylinder length. In this simulation the cylinder radius is fixed at $a = 0.385cm$. It is shown that for relatively short cylinders ($kl_c < 20$) the cross-polarized RCS increases rapidly as its length increases, and the increasing rate becomes gentler for cylinders with $kl_c > 30$.

In the previous simulations, the lower end of the cylinders were placed right above the surface. In the following simulation the effect of the cylinder height location on the scattering interaction between the cylinder and rough surface is considered. Figure 12 shows the cross-polarized RCS (without the direct backscatter from the rough surface) as a function of the height of the vertical cylinder's lower end. It is shown that as the height increases, the RCS increases first, and then become almost a constant function. Note that the rough surface is a distributed target. As the height increases, the area of the illuminated region also increases, thus the RCS does not decrease as the distance between these two target increases.

The sensitivity to the dielectric constants of the cylinder is also examined and the results are shown in Fig. 13. Instead of varying the complex dielectric constant, its corresponding volumetric moisture content is varied. The empirical model [16] is used to calculate the dielectric constants for the chosen moisture content. In Fig. 13, the cross-polarized RCS (only the first term in (41)) is plotted versus the cylinder's volumetric moisture content, while the volumetric moisture content of the surface is kept at 10%. The temperature is assumed to be 23^oC in the calculation of the cylinder's dielectric constant. It is found that the interaction increases as the moisture content (or dielectric constant) increases.

For vertical cylinders, ignoring the cylinder-rough-surface interaction, the main source of the cross-polarized backscatter is the rough surface alone (second-order and higher-order perturbation terms). Fig. 14 compares the cross-polarized backscatter of the rough surface and the rough-surface-cylinder for different values of cylinder number density. These cylinders are

uniformly randomly distributed on the rough surface, and the mutual coupling between them is ignored. While the cross-polarized backscatter from the rough surface ($ks = 0.1$ and $kl = 3.0$) alone decreases rapidly as the incidence angle increases, the backscatter of the composite target increases.

To examine the validity of the scattering formulations, backscatter measurements were performed polarimetrically using the indoor bistatic facilities of the Radiation Laboratory at the University of Michigan. The radar was calibrated polarimetrically using STCT [17]. In these experiments, an X-band stepped frequency radar with the center frequency 9.25 GHz and the bandwidth 1.5 GHz was used. The experimental setup is shown in Fig. 15. A lossy circular cylinder was made by filling a cylindrical cavity in a Styrofoam block with water. The radius and length of the water cylinder were 0.83 cm and 11 cm, respectively. A computer-generated Gaussian random rough surface with $ks = 0.2$ and $kl = 0.9$ was made by milling the surfaces of floral foam blocks, and then they were soaked in water. Independent backscatter measurements were collected by rotating the the rough surface as shown in Fig. 15. Because of the gravity, the water content at the top of the layer was found to be around 30%. The water content is assumed to increase linearly to nearly 100% at 0.5 cm below the top rough layer. The dielectric constant of water calculated from Debye formula was found to be 53.4 + i 39.3.

Figure 16 shows the measured and the theoretical backscattering coefficients of the rough surface without the cylinder. The excellent agreement indicates that the physical parameters and the complete second-order perturbation solution the rough surface are very accurate. Figure 17 shows the measured and theoretical cross-polarized RCS of the rough surface with and without the water cylinder. The inclusion of the cylinder does increase the cross-polarized backscattered field significantly. Note that the interaction of a vertical cylinder with flat surface does not produce any cross-polarized backscatter.

4 Conclusions

In this paper, an electromagnetic scattering solution for the evaluation of the scattering interaction between a dielectric cylinder and a slightly rough surface is presented. Taking the advantage of a newly-developed technique which utilize the reciprocity theorem, the difficulty in formulating the secondary scattered fields from the composite target reduces to the evaluation of integrals involving the scattered fields from the cylinder and polarization currents of the rough surface induced by a plane wave. The scattered field from the cylinder is evaluated in the near-field region using a stationary phase approximation along the cylinder axis. Also the expressions of the polarization current induced within the top rough layer of the rough surface are employed which are derived from the iterative solution of an integral equation. The expression for the scattering matrix of the composite target, which is of interest for modeling of vegetation, are formulated. A sensitivity analysis is performed which shows that the cross-polarized backscatter from the vertical or nearly vertical cylinders is dominated by the scattering interaction between the cylinder and the rough surface. Although the evaluation of the scattering interaction for tilted cylinder is computationally inefficient, it was found that the scattering interaction for cylinders with tilt angle $\beta < 6^\circ$ is approximately the same as that for the cylinder with $\beta = 0^\circ$. The results of the sensitivity analysis indicate that the cross-polarized backscatter generated by the scattering interaction between the cylinder and the rough surface increases with increases in the incidence angle, rms height and correlation length of the rough surface, cylinder radius and length, and dielectric constants of the cylinder and the rough surface. The accuracy of the theoretical formulation is also verified by conducting polarimetric backscatter measurements

from a lossy dielectric cylinder above a slightly rough surface. Excellent agreement between the theoretical prediction and experimental results is obtained.

Acknowledgment: This research was supported by NASA under Contract NAG5-4939 and JPL-958749.

Appendix A

The near-field scattering interaction between two adjacent targets can be evaluated approximately using an iterative approach. It is assumed that the current distribution of an isolated scatterer is the illumination source of the other scatterer and so on. In this appendix it will be shown that the secondary scattered field emanated from target ♯2 ($\mathbf{E}^s_{21}$) can be obtained from the secondary scattered field emanated from target ♯1 ($\mathbf{E}^s_{12}$). Basically, the proof of the relationship between $\bar{\bar{\mathbf{S}}}^{cr}$ and $\bar{\bar{\mathbf{S}}}^{rc}$ as given in (31) is presented. Without loss of generality, consider two adjacent targets in free space illuminated by a plane wave. Suppose the induced current on (or within) target ♯1 in the absence of target ♯2 is given by $\mathbf{J}_1(\mathbf{r}_1)$, then the scattered field generated by this current can be computed from

$$\mathbf{E}^s_1 = ik_oZ_o\int_{V_1}\bar{\bar{\mathbf{G}}}(\mathbf{r},\mathbf{r}'_1)\mathbf{J}_1(\mathbf{r}'_1)\,dv'_1 = \frac{-k_oZ_o}{8\pi^2}\iint\frac{1}{k_z}\left(\bar{\bar{I}}-\hat{k}\hat{k}\right)\int_{V_1}\mathbf{J}_1(\mathbf{r}'_1)e^{ik_o\hat{k}\cdot(\mathbf{r}-\mathbf{r}')}dv'd\mathbf{k}_\perp \tag{A.1}$$

where the second equality is resulted from the application of the Fourier Transform of the dyadic Green's function $\bar{\bar{\mathbf{G}}}$. If the observation point $\mathbf{r}$ is significantly apart from V_1, most contribution of the spectral integrand for calculation of $\mathbf{E}^s_1$ come from values of $\mathbf{k}_\perp$ for which k_z and these $\hat{k}$ are real quantities. In this case, it is recognized that

$$\mathbf{E}^s(\hat{k},\hat{k}_i) = \frac{ik_oZ_oe^{ik_or}}{4\pi r}\left(\bar{\bar{I}}-\hat{k}\hat{k}\right)\int_{V_1}\mathbf{J}_1(\mathbf{r}'_1)e^{-ik_o\hat{k}\cdot\mathbf{r}'}dv' \tag{A.2}$$

is the bistatic scattering far-field of target ♯1 with the incident and scattering directions along $\hat{k}_i$ and $\hat{k}$, respectively. Also noting that this scattered field can be written as

$$\mathbf{E}^s(\hat{k},\hat{k}_i) = \frac{e^{ik_or}}{r}e^{ik_o(\hat{k}_i-\hat{k})\cdot\mathbf{r}_{c1}}\bar{\bar{\mathbf{S}}}_1(\hat{k},\hat{k}_i)\mathbf{E}^{\mathbf{i}}\ , \tag{A.3}$$

where $\bar{\bar{\mathbf{S}}}_1(\hat{k},\hat{k}_i)$ is the bistatic scattering matrix of target ♯1 and $\mathbf{r}_{c1}$ is a vector representing the location of target ♯1.

Therefore the scattered field given by (A.1) can be written as

$$\mathbf{E}^s_1 = \left\{\frac{i}{2\pi}\iint\frac{1}{k_z}\bar{\bar{\mathbf{S}}}_1(\hat{k}_i,\hat{k})e^{ik_o(\hat{k}_i-\hat{k})\cdot\mathbf{r}_{c1}}e^{ik_o\hat{k}\cdot\mathbf{r}}d\mathbf{k}_\perp\right\}\mathbf{E}^{\mathbf{i}}\ . \tag{A.4}$$

In this representation the near-field scattered from target ♯1 is expanded in terms of a spectrum of plane waves. Using $\mathbf{E}^s_1$ as the illuminating field the secondary scattered field in the far-field region can be computed from

$$\begin{aligned}\mathbf{E}^s_{21} &= \frac{e^{ik_or}}{r}\left\{\frac{i}{2\pi}\iint\frac{1}{k_z}\bar{\bar{\mathbf{S}}}_2(\hat{k}_s,\hat{k})\bar{\bar{\mathbf{S}}}_1(\hat{k},\hat{k}_i)e^{ik_o(\hat{k}_i-\hat{k})\cdot\mathbf{r}_{c1}}e^{ik_o(\hat{k}-\hat{k}_s)\cdot\mathbf{r}_{c2}}d\mathbf{k}_\perp\right\}\mathbf{E}^{\mathbf{i}}\\ &= \frac{e^{ik_or}}{r}\bar{\bar{\mathbf{S}}}_{21}(\hat{k}_s,\hat{k}_i)\mathbf{E}^{\mathbf{i}}\ ,\end{aligned} \tag{A.5}$$

where $\bar{\bar{\mathbf{S}}}_2(\hat{k}_s,\hat{k})$ is the bistatic scattering matrix of target ♯2 and $\mathbf{r}_{c2}$ is the vector position of target ♯2. in a similar manner $\mathbf{E}^s_{12}$ can be obtained and is given by

$$\begin{aligned}\mathbf{E}^s_{12} &= \frac{e^{ik_or}}{r}\left\{\frac{i}{2\pi}\iint\frac{1}{k_z}\bar{\bar{\mathbf{S}}}_1(\hat{k}_s,-\hat{k})\bar{\bar{\mathbf{S}}}_2(-\hat{k},\hat{k}_i)e^{ik_o(-\hat{k}-\hat{k}_s)\cdot\mathbf{r}_{c1}}e^{ik_o(\hat{k}_i+\hat{k})\cdot\mathbf{r}_{c2}}d\mathbf{k}_\perp\right\}\mathbf{E}^{\mathbf{i}}\\ &= \frac{e^{ik_or}}{r}\bar{\bar{\mathbf{S}}}_{12}(\hat{k}_s,\hat{k}_i)\mathbf{E}^{\mathbf{i}}\ .\end{aligned} \tag{A.6}$$

Now it can easily be shown that $\bar{\bar{S}}_{12}(\hat{k}_s, \hat{k}_i) = \bar{\bar{S}}_{21}^{(-t)}(-\hat{k}_i, -\hat{k}_s)$, since according to reciprocity theorem (using the forward scattering alignment [9])

$$\bar{\bar{S}}_1(\hat{k}_s, \hat{k}) = \bar{\bar{S}}_1^{(-t)}(-\hat{k}, -\hat{k}_s) \ .$$
$$\bar{\bar{S}}_2(\hat{k}, \hat{k}_i) = \bar{\bar{S}}_2^{(-t)}(-\hat{k}_i, -\hat{k}) \ .$$

In the backscattering direction, $\hat{k}_s = -\hat{k}_i$, and therefore $\bar{\bar{S}}_{12}(-\hat{k}_i, \hat{k}_i) = \bar{\bar{S}}_{21}^{(-t)}(-\hat{k}_i, \hat{k}_i)$ as stated in (31).

References

[1] Ulaby, F.T., K. Sarabandi, K. McDonald, M. Whitt, and M.C. Dobson, "Michigan microwave canopy scattering model," *Int. J. Remote Sensing*, vol. 11, no. 7, pp. 2097-2128, 1990.

[2] Tsang, L., J. Kong, and R.T. Shin, *Theory of Microwave Remote Sensing*, John Wiley and Sons, New York, 1985.

[3] Sarabandi, K., P.F. Polatin, and F.T. Ulaby, "Monte-Carlo simulation of scattering from a layer of vertical cylinders," *IEEE Trans. Antennas Propagat.*, vol. 41, no. 4, pp. 465-474, 1993.

[4] Sarabandi, K. and P.F. Polatin, "Electromagnetic scattering from two adjacent objects," *IEEE Trans. Antennas Propagat.*, vol. 42, no. 4, pp. 510-517, 1994.

[5] Hsu C.C., H.C. Han, R.T. Shin, J.A. Kong, A. Beaudin, and T. LE Toan, "Radiative transfer theory theory for polarimetric remote sensing of pine forest at P band," *Int. J. Remote Sensing,* vol. 15, no. 14, pp. 2943-2954, 1994.

[6] Lin, Y.C. and K. Sarabandi, "A Monte-Carlo coherent scattering model for forest canopies using fractal generated trees," Submitted for publication in *IEEE Trans. Geosci. Remote Sensing.*

[7] Durden, S.L., J.J. van Zyl, and H.A. Zebker, "Modeling and Observation of the Radar Polarization Signature of Forested Areas," *IEEE Trans. Geosci. Remote Sensing*, vol. 27, no. 3, pp. 290-301, 1989.

[8] Polatin P.F., K. Sarabandi, and F.T. Ulaby, "Monte-Carlo simulation of electromagnetic scattering from a layer of vertical cylinders," *IEEE Trans. Antennas Propagat.*, vol. 43, no. 10, pp. 1048-1057, Oct. 1995.

[9] Ulaby, F.T. and C. Elachi, *Radar Polarimetry for Geoscience Applications,* Artech House, Inc., Norwood, MA, 1990.

[10] Sarabandi, K. and T. Chiu, "Electromagnetic scattering from slightly rough surface with inhomogeneous dielectric profiles," *IEEE Trans. Antennas Propagat.*, vol. 45, no. 9, pp. 1419-1430, Sep. 1997.

[11] Rice S.O., "Reflection of electromagnetic wave by slightly rough surface," *Communication in Pure and Applied Mathematics.*, vol. 4, pp. 351-378, 1951.

[12] Chiu, T., *Electromagnetic Scattering from Short Branching Vegetation*, Ph.D. dissertation, the University of Michigan, Ann Arbor, 1998.

[13] Seker S.S. and A. Schneider, "Electromagnetic Scattering from a dielectric cylinder of finite length," *IEEE Trans. Antennas Propagat.*, vol. 36, no. 2, pp. 303-307, Feb. 1988.

[14] Harrington, R.F., *Time-Harmonic Electromagnetic Fields*, McGraw-Hill, Inc., NY, 1961.

[15] Hallikainen, M.T., F.T. Ulaby, M.C. Dobson, M.A. El-Rayes, and L. Wu, "Microwave dielectric behavior of wet soil — part I: empirical models and experimental observations," *IEEE Trans. Geosci. Remote Sensing*, vol. GE-23, no. 1, pp. 25-34, January 1985.

[16] Ulaby F.T. and M.A. El-Rayes, "Microwave dielectric spectrum of vegetation — part II: dual-dispersion model," *IEEE Trans. Geosci. Remote Sensing*, vol. GE-25, no. 5, pp. 550-557, September 1987.

[17] Sarabandi, K. and F.T. Ulaby, "A convenient technique for polarimetric calibration of radar systems," *IEEE Trans. Geosci. Remote Sensing*, vol. 28, pp. 1022-1033, 1990.

[18] Chiu T., K. Sarabandi, and F.T. Ulaby, "Polarimetric backscattering measurement of herbaceous vegetation: a sensitivity study for soil moisture retrieval." In *Proceedings of the International Geoscience and Remote Sensing Symposium*, Lincoln, Nebraska, USA, May 1996.

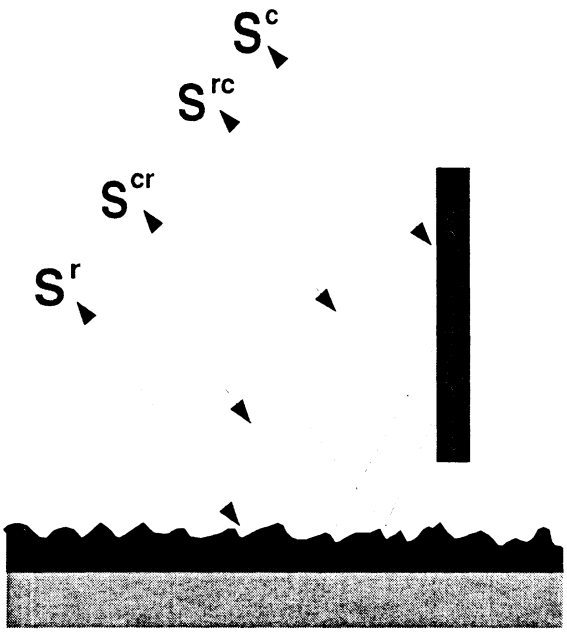

Figure 1: Configuration of the scattering problem.

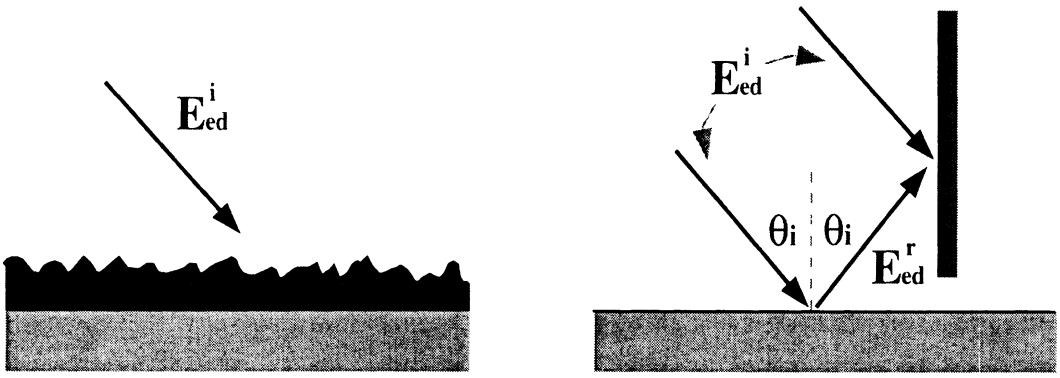

(a) (b)

Figure 2: The target is decomposed into two isolated targets above a half-space dielectric: (a) a rough layer of dielectric and (b) a dielectric cylinder.

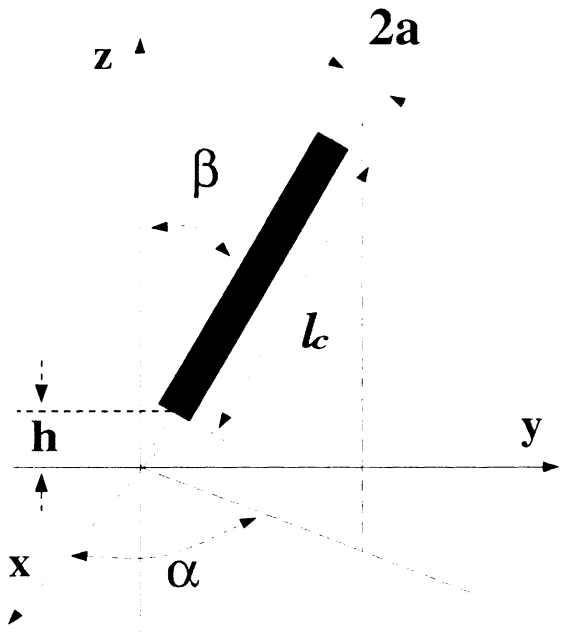

Figure 3: The parameters indicating the dimensions and orientation angles for a cylinder.

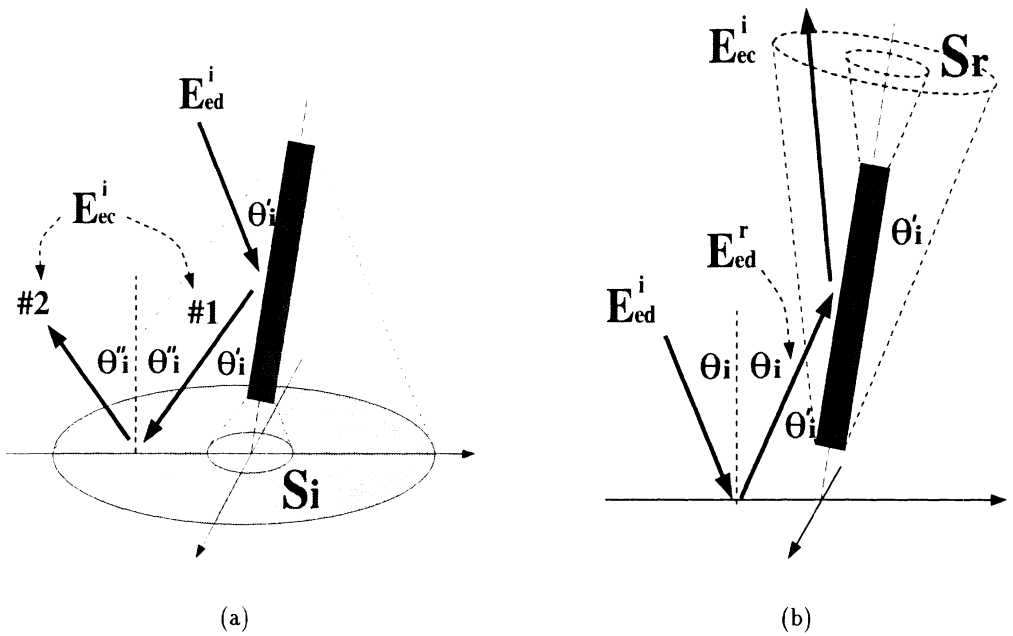

Figure 4: The conical regions of the significant scattered field from a cylinder for the direct incident fields $\mathbf{E}^i_{ed}$ (a) and the reflected incident field $\mathbf{E}^r_{ed}$ (b).

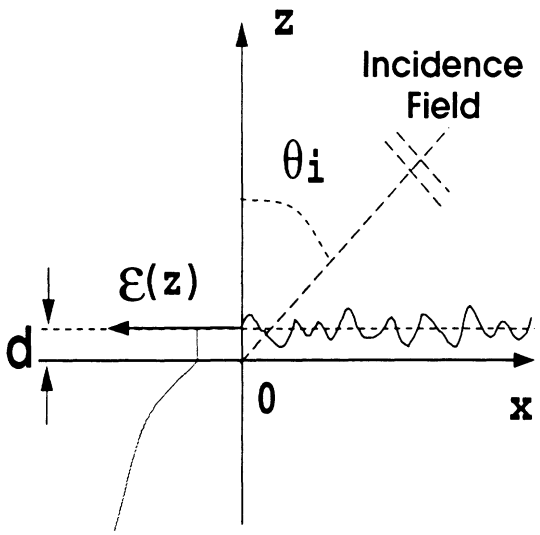

Figure 5: An inhomogeneous half-space medium with a rough interface. Left side of this figure shows the dielectric profile.

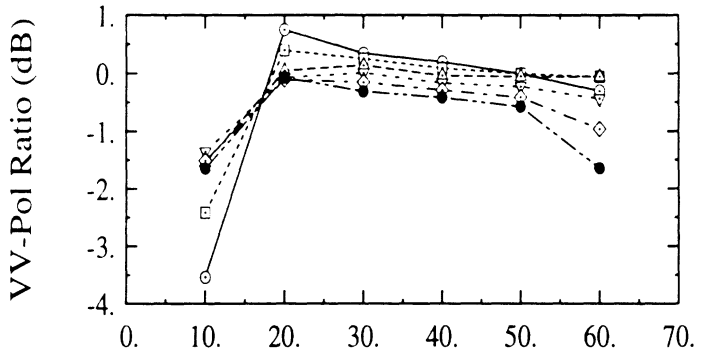

(a)

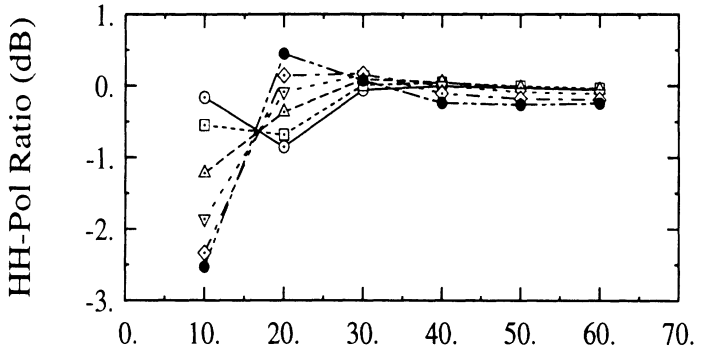

(b)

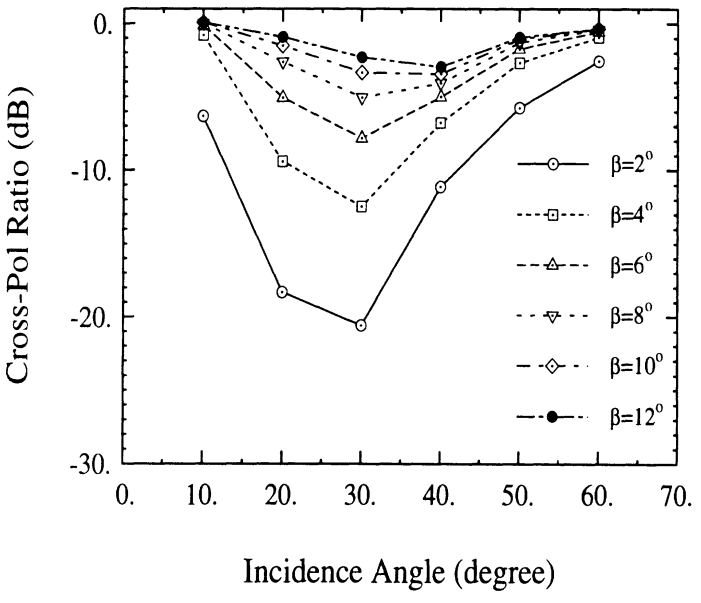

(c)

Figure 6: The RCS ratios of the zeroth-order to the complete first-order for (a) vv-polarized, (b) hh-polarized, and (c) cross-polarized backscatter and for different cylinder tilt angles. The simulation is carried out for a surface with $ks = 0.1$ and $kl = 2.0$.

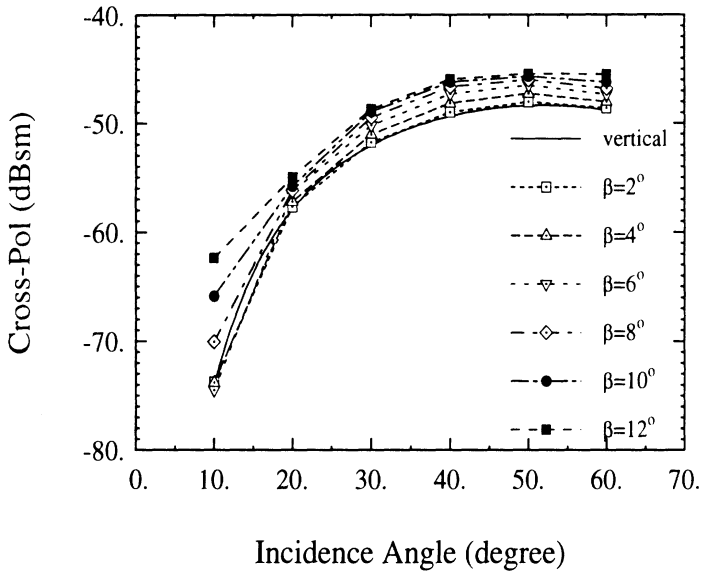

Figure 7: The cross-polarized RCS caused by the interaction between a cylinder ($a = 0.385cm$, $l_c = 0.71m$, and $\epsilon_c = 43.4 + i13.2$) and a rough surface ($ks = 0.1$, $kl = 3.0$, and $\epsilon_g = 4.9 + i0.9$).

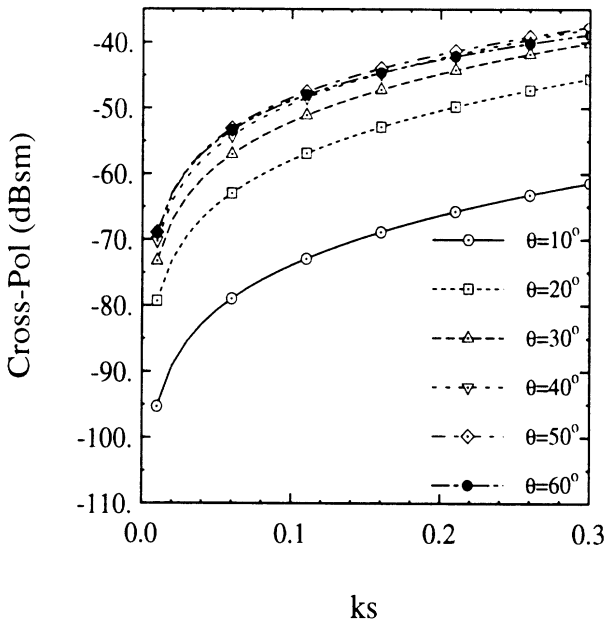

Figure 8: The cross-polarized RCS of the cylinder-rough surface composite target versus ks of the rough surface ($a = 0.385cm$, $l_c = 0.71m$, $\epsilon_c = 43.4 + i13.2$, $kl = 3.0$, and $\epsilon_g = 4.9 + i0.9$).

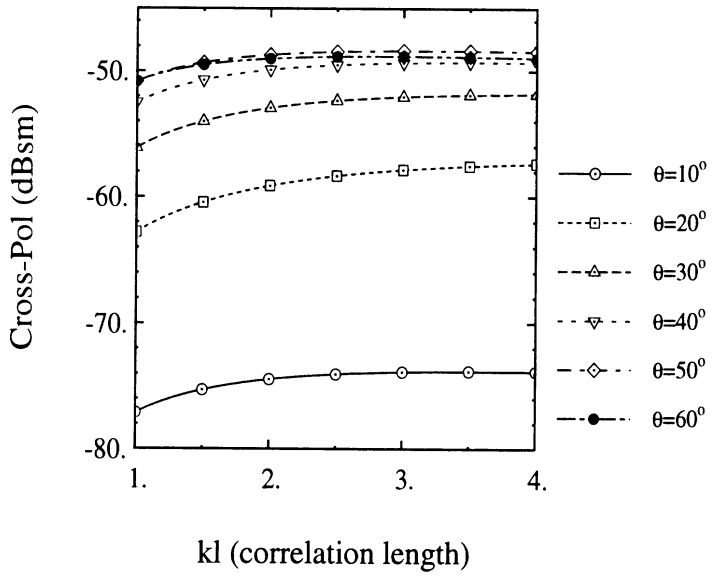

Figure 9: The cross-polarized RCS of the cylinder-rough surface composite target versus kl of the rough surface ($a = 0.385cm$, $l_c = 0.71m$, $\epsilon_c = 43.4 + i13.2$, $ks = 1.0$, and $\epsilon_g = 4.9 + i0.9$).

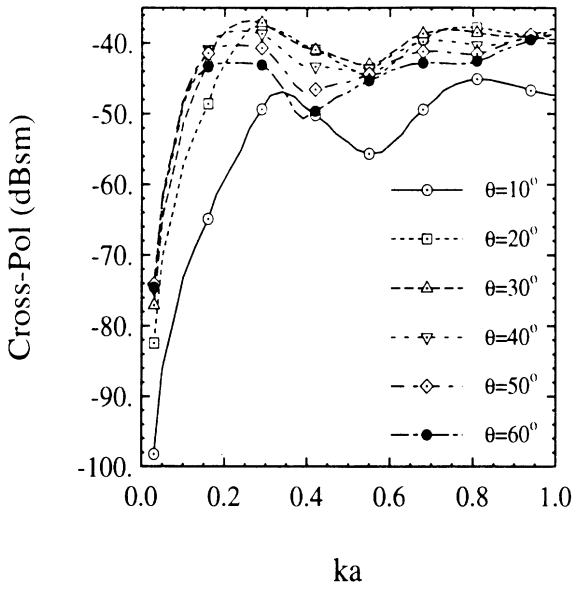

Figure 10: The cross-polarized RCS of the cylinder-rough surface composite target versus the radius of the vertical cylinder ($l_c = 0.71m$, $\epsilon_c = 43.4 + i13.2$, $ks = 0.1$, $kl = 3.0$, and $\epsilon_g = 4.9 + i0.9$).

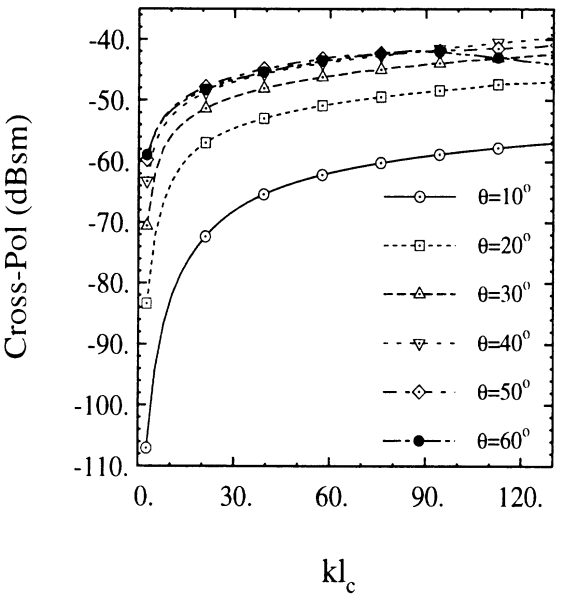

Figure 11: The cross-polarized RCS of the cylinder-rough surface composite target versus the length of the vertical cylinder ($a = 0.385cm$, $\epsilon_c = 43.4 + i13.2$, $ks = 0.1$, $kl = 3.0$, and $\epsilon_g = 4.9 + i0.9$).

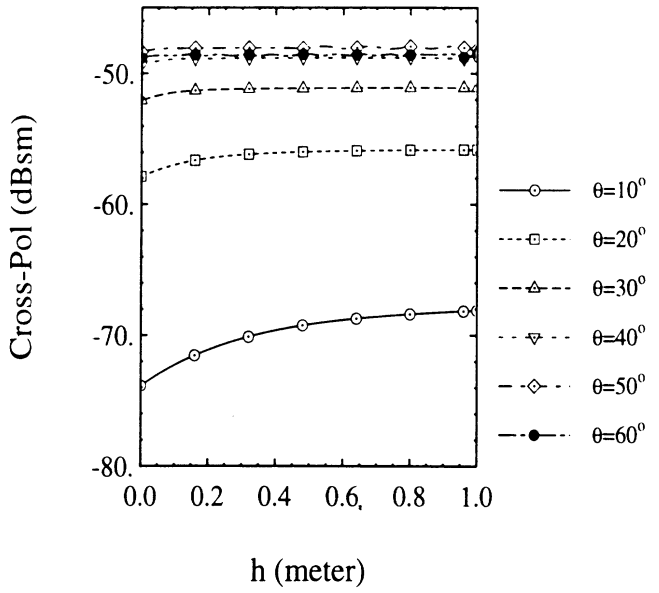

Figure 12: The cross-polarized RCS of the cylinder-rough surface composite target versus the height of the cylinder lower end above the ground ($a = 0.385cm$, $l_c = 0.71m$, $\epsilon_c = 43.4 + i13.2$, $ks = 0.1$, $kl = 3.0$, and $\epsilon_g = 4.9 + i0.9$).

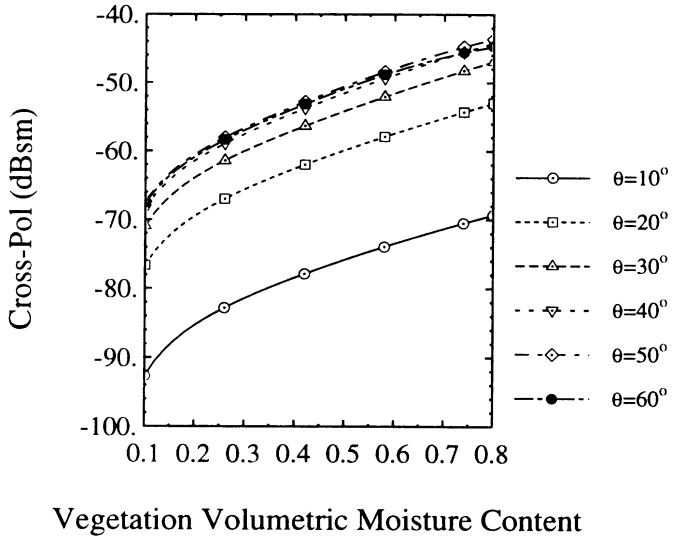

Figure 13: The cross-polarized RCS of the cylinder-rough surface composite target versus the volumetric moisture content of the vertical cylinder ($a = 0.385cm$, $l_c = 0.71m$, $ks = 0.1$, $kl = 3.0$, and $\epsilon_g = 4.9 + i0.9$).

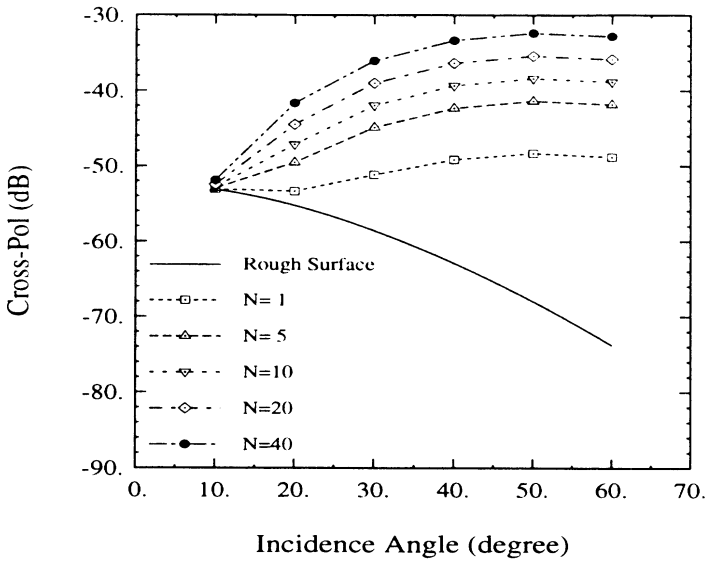

Figure 14: A comparison of the cross-polarized backscatter of the vertical cylinder-rough surface composite target to that of the rough surface along. The RCS is plotted as a function of incidence angle and number density. The direct backscattering from rough surface alone (σ_{pq}^0) is also plotted for comparison ($a = 0.385cm$, $l_c = 0.71m$, $\epsilon_c = 43.4 + i13.2$, $ks = 0.1$, $kl = 3.0$, and $\epsilon_g = 4.9 + i0.9$).

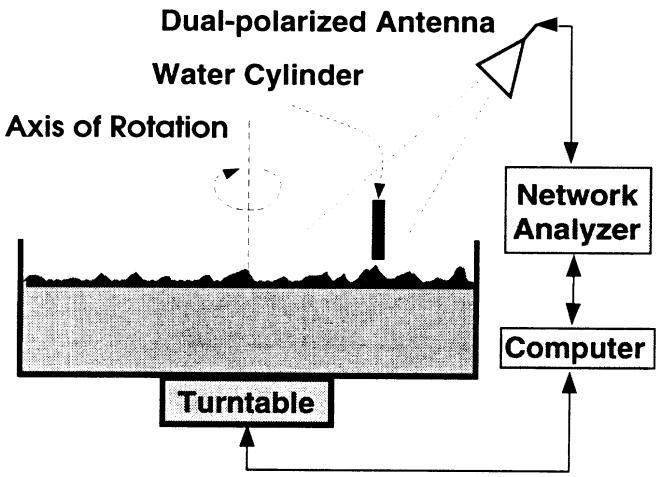

Figure 15: The experimental setup for the backscatter measurement of a vertical cylinder above a rough ground plane.

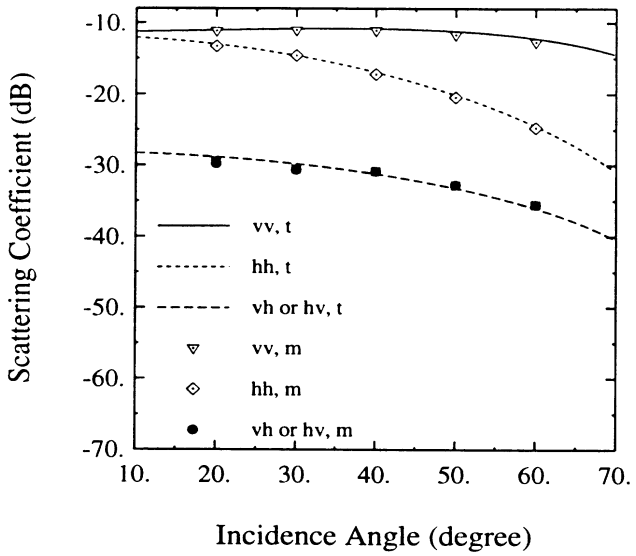

Figure 16: The backscattering coefficients of the rough surface with $ks = 0.2$ and $kl = 1.0$ at 9.25 GHz.

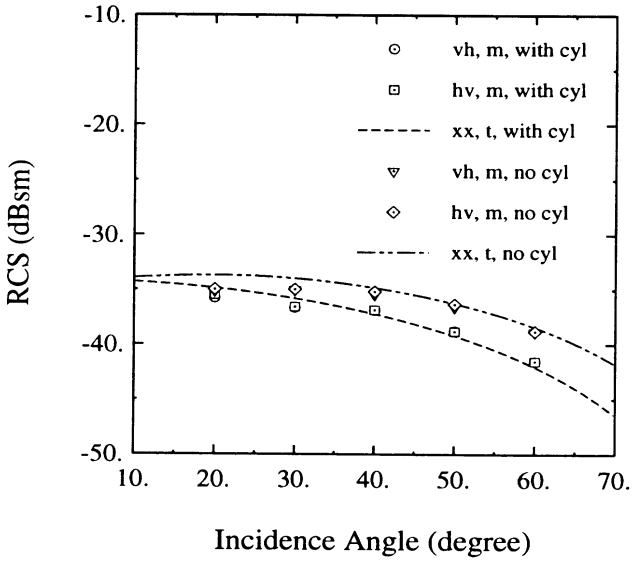

Figure 17: The cross-polarized RCS of a water cylinder with $a = 0.83cm$ and $l_c = 11.0cm$ above the rough surface at 9.25 GHz. The RCS of the rough surface alone ($\sigma^0_{pq}A$) is also shown for comparison.